DOI: 10.1002/chem.201100218

Structure, Magnetism and Theory of a Family of Nonanuclear $Cu^{II}_5Ln^{III}_4$–Triethanolamine Clusters Displaying Single-Molecule Magnet Behaviour

Stuart K. Langley,[a] Liviu Ungur,[b] Nicholas F. Chilton,[a] Boujemaa Moubaraki,[a] Liviu F. Chibotaru,[b] and Keith S. Murray*[a]

Abstract: Synthesis, crystal structures and magnetic studies are reported for four new heterometallic Cu^{II}–Ln^{III} clusters. The reaction of $Cu(NO_3)_2{\cdot}3H_2O$ with triethanolamine ($teaH_3$), pivalic acid, triethylamine and $Ln(NO_3)_3{\cdot}6H_2O$ (Ln = Gd, Tb, Dy and Ho) results in the formation of four isostructural nonanuclear complexes of general formula $[Cu^{II}_5Ln^{III}_4O_2(teaH)_4\{O_2CC(CH_3)_3\}_2(NO_3)_4(OMe)_4]{\cdot}2MeOH{\cdot}2Et_2O$ [Ln = Gd (**1**), Tb (**2**), Dy (**3**) and Ho (**4**)]. The metal core of each cluster is made up of four face- and vertex-sharing tetrahedral units. Solid-state DC magnetic susceptibility studies reveal competing anti- and ferromagnetic interactions within each cluster leading to large-spin ground states for **1**–**4**. Solid-state AC magnetic susceptibility studies show frequency-dependent out-of-phase (χ''_M) signals for **2**–**4** below 4 K, suggestive of single-molecule magnet behaviour. Ab initio calculations on one of the anisotropic examples (**3**) provided a rare set of *J* values for Dy–Cu and Cu–Cu exchange interactions (Dy–Dy zero), some ferro- and some antiferromagnetic in character, that explain its magnetic behaviour.

Keywords: cluster compounds · copper · lanthanides · magnetic properties · N,O ligands

Introduction

The search for new single-molecule magnets (SMMs)[1] has led to an exponential growth of polynuclear metal clusters, in which single-molecule magnetic properties are often observed. SMMs derive their properties from having a large ground spin state (*S*) with a sufficiently large magnetic anisotropy due to a negative axial zero-field splitting (*D*). This leads to an appreciable barrier ($U_{eff} = S^2|D|$) for magnetization reversal and thus at sufficiently low temperatures these clusters will act as nanoscale magnets. These observations have led chemists to search for a variety of synthetic strategies to obtain various types of metal clusters with the above parameters. The main route to SMMs thus far has been the isolation of homo- and mixed-valent manganese clusters, usually derived from treatment of simple mono- or polynuclear building blocks with various bridging ligands.[2] This self-assembly technique has also been successfully used to isolate SMMs with other 3d transition metals, such as iron,[3] cobalt[4] and nickel[5] and has also been extended to heterometallic Mn-3d clusters.[6] The largest energy barrier found for transition-metal clusters obtained by this method is that of a Mn^{III}_6 compound with a barrier to magnetisation reversal of $U_{eff} = 86.4$ K.[7] More recently SMM behaviour had also been observed in various lanthanide clusters,[8] as well as in clusters composed of a combination of 3d and 4f ions.[9] The use of lanthanide ions in cluster formation has led to reports of increased anisotropy barriers, observed for Dy_4,[10a] Dy_4[10b] and Dy_6[10c] compounds, with U_{eff} values of 170, 173 and 200(10) K, respectively. This promising observation of improved U_{eff} values for pure Ln clusters may also translate to heterometallic 3d–4f systems, in which one can exploit the large spin and anisotropy of the transition-metal and lanthanide ions, respectively.

A sub-area of 3d–4f cluster chemistry uses Cu^{II} with the more anisotropic lanthanides (Tb, Dy and Ho), which can give rise to an Ising-type magnetoanisotropy needed for SMM behaviour. This chemistry was initially developed from the observation that the magnetic interactions between Cu^{II} ions and isotropic Gd^{III} ions were often ferromagnetic[11] giving rise to clusters with large-spin (*S*) ground states. This led to studies by Kahn et al.,[12] for example, that concluded that the Cu^{II}–Tb^{III} and Cu^{II}–Dy^{III} interactions, albeit weak in magnitude, were also generally ferromagnetic, whereas the Cu^{II}–Ho^{III} interaction has been found to be either anti- or ferromagnetic. The orbital contribution and ligand-field effects present with the Tb^{III}, Dy^{III} and Ho^{III} ions, however, complicate the theoretical analysis of the variable-temperature (and -field) magnetic susceptibilities and this still poses a problem in this area of spin-coupled cluster chemistry. A simple magnetic analysis could be obtained in

[a] Dr. S. K. Langley, N. F. Chilton, Dr. B. Moubaraki, Prof. K. S. Murray
School of Chemistry, Monash University
Clayton, Victoria, 3800
Fax: (+61) 399054512
E-mail: keith.murray@monash.edu

[b] Dr. L. Ungur, Prof. L. F. Chibotaru
Department of Quantum and Physical Chemistry
Institution of Nanoscale Physics and Chemistry
Katholieke Universiteit Leuven
Celestijnenlaan 200F, 3001 Heverlee (Belgium)

Supporting information for this article is available on the WWW under http://dx.doi.org/10.1002/chem.201100218.

some cases, as in the work by Kahn et al.[12] utilizing diamagnetic ions in place of the copper ions, which allowed the sign of the exchange interaction to be determined. This was done by comparing the magnetic properties of isostructural Ln^{III}–Cu^{II} and Ln^{III}–Zn^{II} compounds, in which the deviation in the magnetic susceptibility in the Zn^{II} case is due to population of the Ln^{III} Stark energy levels. Transferring this information to the magnetic properties of the Ln^{III}–Cu^{II} compound may result in the determination of the Cu–Ln interaction.

More rigorous fitting of magnetic data for 3d–4f combinations in dinuclear family $[Ln^{III}Cu^{II}(sal)(NO_3)_2(L)(MeOH)]$ (Ln^{III} = Tb, Dy, Ho, Er; sal^- = salicylaldehydato; L = vanillin-derived Schiff base chelate)[13a] utilised a Hamiltonian containing isotropic spin–spin interactions, Zeeman splitting and ligand-field terms of type B_2^0, B_4^0 and B_6^0 to calculate the ground J_z Ln^{III} Stark multiplets and obtain J_{Cu-Ln} from the splitting of the lowest level (ca. −25 K). Crystallites of these easy-axis materials were oriented in the DC field so that anisotropy in the observed $\chi_M T$ values allowed the ligand-field parameters to be delineated.

Several other types of heterometallic Cu^{II}–Ln^{III} clusters are known. Early work by Winpenny et al.,[14] for example, produced a number of Cu^{II}–Ln^{III} compounds with pyridonate ligands, whereas SMMs were recently reported for dinuclear CuTb,[13b,c,d] trinuclear $CuDy_2$[15] and several tetranuclear Cu_2Ln_2 (Ln = Dy and Tb) compounds.[16] Larger clusters such as $CuDy_4$,[17] $\{Cu_3Dy_3\}_2$,[18] Cu_6Dy_3[19] and $Cu_{24}Dy_8$[20] also display SMM behaviour. It is therefore apparent that heterometallic Cu–Ln clusters display SMM behaviour due to a combination of large-spin ground states, which are often observed, and a large anisotropy derived from the lanthanide ions. Although there are other examples of non-SMM Cu–Ln clusters,[21] this area of chemistry has not been researched as extensively as other cluster types, with only a limited analysis performed on the magnetic data for many of these compounds.

We have recently been investigating the potential of the polydentate ligand triethanolamine ($teaH_3$) to form polynuclear 3d transition-metal[22] Mn–4f[23] and lanthanide-only clusters,[8e] and have now extended such studies into Cu–Ln systems. During our previous work with $teaH_3$, we showed that the cluster topology is highly dependent on the co-ligand used[22b] and here we have chosen pivalic acid as the co-ligand. We report the synthesis and magnetic properties of four isostructural Cu–Ln clusters of general formula $[Cu^{II}_5Ln^{III}_4O_2(teaH)_4\{O_2CC(CH_3)_3\}_2(NO_3)_4(OMe)_4]$·2MeOH·2$Et_2O$ [Ln = Gd (**1**), Tb (**2**), Dy (**3**) and Ho (**4**)]. These compounds display new, attractive cluster structures and interesting magnetic features. Detailed ab initio calculations on $Cu^{II}_5Dy^{III}_4$ cluster **3**, using methods and programs recently described for SMM clusters such as $[Cr^{III}_4Dy^{III}_4(\mu_3\text{-}OH)_4(\mu\text{-}N_3)_4(mdea)_4(piv)_4]$·3$CH_2Cl_2$ (mdea = methyldiethanolamine dianion, piv = pivalate),[24] yielded a set of isotropic coupling constants for Dy–Cu and Cu–Cu pathways that simulate well the susceptibility data. In a separate collaboration, Cu–Gd compound (**1**) has been shown to have a record value for the magnetocaloric effect (MCE) at low temperatures, compared to other spin-coupled molecular clusters.[25]

Results and Discussion

Structural descriptions: $[Cu^{II}_5Ln^{III}_4O_2(teaH)_4\{O_2CC(CH_3)_3\}_2(NO_3)_4(OMe)_4]$·2MeOH·2$Et_2O$ [Ln = Gd (**1**), Tb (**2**), Dy (**3**) and Ho (**4**)]. Compounds **1**, **2**, **3** and **4** (Figure 1) crystallize in the triclinic space group $P\bar{1}$ (Table 1) with the asymmetric unit containing half the cluster, which lies upon an inversion centre. Each complex is isostructural and contains five Cu^{II} (Cu1–Cu3 and symmetry equivalents) and four Ln^{III} (Ln1, Ln2 and symmetry equivalents) ions. Compounds **1**–**4** have

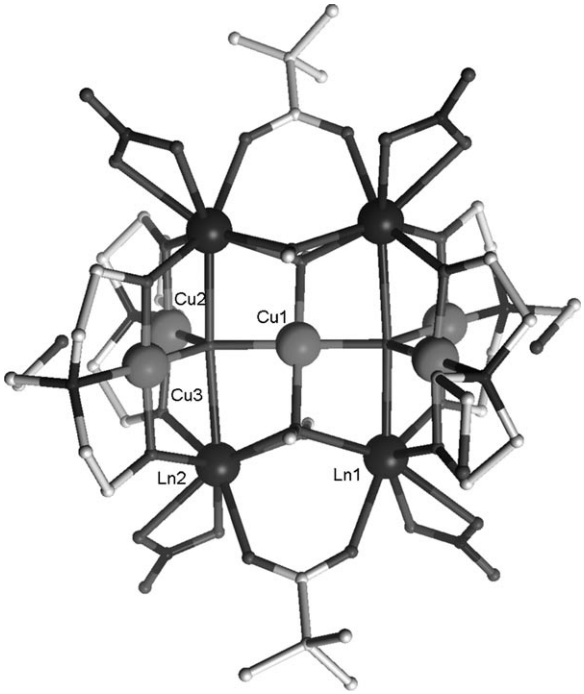

Figure 1. Weblab viewer representation of **1**–**4**. Cu^{II}: grey balls; Ln^{III}: black balls.

a planar arrangement of Cu^{II} ions, which form a bow-tie arrangement, with the four Ln^{III} ions forming a rectangle that lies above and below the plane of the Cu^{II} ions (Figure 2, left). Overall this affords a metal core of four face- and vertex-sharing tetrahedral units (Figure 2, right). The average Ln···Ln distances in **1**–**4** are 3.71 and 5.26 Å (Ln1···Ln2 and Ln1···Ln2', respectively, and their symmetry equivalents). The average Cu···Ln distances between the outer Cu^{II} sites (Cu2 and Cu3 and symmetry equivalents) and the Ln^{III} ions is 3.29 Å, whereas the distance of the central Cu^{II} ion to the Ln^{III} ions is 3.22 Å. The average Cu···Cu distance between the outer Cu^{II} sites is 3.114 Å, whereas the average central-to-outer Cu···Cu distance is 3.46 Å. The metal core observed in **1**–**4** is similar to those of previously reported Ln_4Cu complexes (Ln = Nd, Gd and Dy) in which a single

Table 1. Crystallographic data for complexes **1–4**.

	1	**2**	**3**	**4**
formula[a]	$Cu_5Gd_4C_{48}H_{110}O_{38}N_8$	$Cu_5Tb_4C_{48}H_{110}O_{38}N_8$	$Cu_5Dy_4C_{48}H_{110}O_{38}N_8$	$Cu_5Ho_4C_{48}H_{110}O_{38}N_8$
M_r [g mol^{-1}]	2354.16	2360.82	2375.14	2384.88
crystal system	triclinic	triclinic	triclinic	triclinic
space group	$P\bar{1}$	$P\bar{1}$	$P\bar{1}$	$P\bar{1}$
a [Å]	11.050(2)	11.0443(4)	11.080(2)	11.087(2)
b [Å]	13.830(3)	13.8090(5)	13.820(3)	13.803(3)
c [Å]	14.030(3)	14.0113(5)	13.990(3)	13.985(3)
α [°]	78.80(3)	78.935(2)	78.90(3)	78.94(3)
β [°]	83.81(3)	83.743(2)	84.10(3)	84.10(3)
γ [°]	69.28(3)	69.405(2)	69.04(3)	69.05(3)
V [Å^{-13}]	1965.4(8)	1961.12(12)	1961.7(7)	1960.3(7)
T [K]	100(2)	123(2)	100(2)	100(2)
Z	1	1	1	1
ρ_{calcd} [g cm^{-3}]	1.989	1.999	2.011	2.020
λ[b] [Å]	0.71082	0.71073	0.77512	0.71253
data measured	12139	27457	21274	24425
indep reflns	7056	8661	5521	6300
R_{int}	0.0315	0.0393	0.0456	0.1413
reflns with $I>2\sigma(I)$	6876	6995	5520	6093
parameters	477	477	507	506
restraints	0	25	29	52
$R1$[c], $wR2$[c]	0.0398, 0.099	0.045, 0.1	0.039, 0.1083	0.0645, 0.1685
GOF	1.132	1.087	1.041	1.080
largest residuals [e Å^{-3}]	1.09, −1.331	1.539, −1.09	1.49, −1.53	1.53, −1.74

[a] Including molecules of solvation. [b] Graphite monochromator. [c] $R1=\Sigma||F_o|-|F_c||/\Sigma|F_o|$, $wR2=[\Sigma[w(F_o^2-F_c^2)^2]/\Sigma[w(F_o^2)^2]]^{1/2}$.

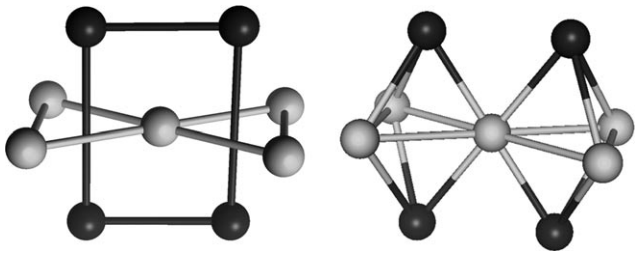

Figure 2. Right: The face- and vertex-sharing tetrahedral core and left: the rectangle within a bow tie of **1–4**. Cu^{II}: grey balls; Ln^{III}: black balls.

central Cu^{II} site is surrounded by a rectangular array of Ln^{III} ions.[17] In that study, the magnetic behaviour of each Ln_4Cu core revealed large-spin ground states, and SMM behaviour was found for the Dy^{III} case.[17b]

The magnetic skeletons of **1–4** are stabilized primarily by two μ_5-oxido ligands, which bond to all ions in the cluster and by four methoxide ligands, which display two modes of bonding. Two adopt a μ_2 bonding mode and bridge Ln1 to Ln2 (and symmetry-equivalent ions) across a rectangular edge, whereas two μ_3-MeO^- ligands bridge Ln1 to Ln2 (and to the symmetry-equivalent ions) and to the central Cu^{II} ion (Cu1). The clusters are further stabilized around the periphery by bridging pivalate and doubly deprotonated triethanolamine ($teaH^{2-}$) ligands, as well as by terminal nitrate ions. The two pivalate ligands bridge Ln1 and Ln2 (and symmetry equivalents) in the usual *syn,syn* mode. In **3** and **4** the $(CH_3)_3$ group is disordered over two positions. The four $teaH^{2-}$ ligands adopt a μ_3:η^2:η^2:η^1:η^0 mode of bonding; each bonds through the N atom to one of Cu2, Cu3, Cu2a and Cu3a and bridges through two μ_2-O atoms from a outer Cu^{II} ion to a Ln^{III} ion. The non-bonding alcohol arms on the four $teaH^{2-}$ ligands remain protonated. Two of them lie in an axial position above the outer Cu^{II} ions and form hydrogen bonds to MeOH solvent molecules. The remaining two arms form intermolecular hydrogen bonds to nitrate ions of adjacent clusters, generating 1D inter-cluster hydrogen-bonded chains (Figure 3). The four terminal nitrate ions each chelate one of the four Ln^{III} ions. For **1–4** the central Cu^{II} ion (Cu1) and the outer four Cu^{II} ions (Cu2, Cu3 and symmetry equivalents) are four-coordinate with square-planar geometries. At these sites there are also addi-

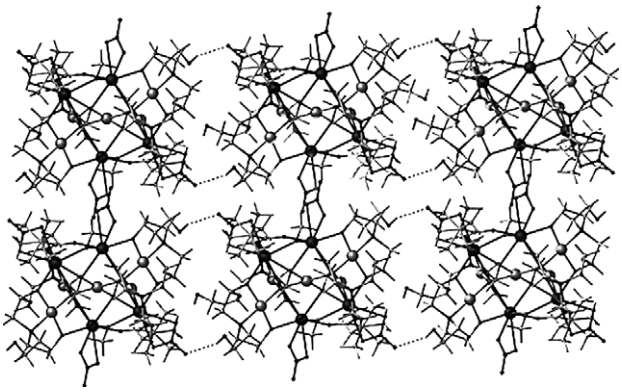

Figure 3. Inter-cluster hydrogen-bonding interactions (dashed lines) forming 1D chains in **1–4**.

tional long (axial) contacts present within each cluster. Cu1 has two long axial contacts through the two μ_2-methoxide ligands, with an average distance of 2.67 Å (for **1–4**). Cu2 has one long contact to a non-bonded O atom of a $teaH^{2-}$ ligand, whereas Cu3 also has a long contact to the same atom, with average Cu···O distances of 2.74 and 2.44 Å, respectively (for **1–4**). The average Cu–L bond length (square-planar) for **1–4**, is 1.94, 1.94, 1.95 and 1.94 Å, respectively. Each Ln^{III} site is eight-coordinate with distorted square-antiprismatic geometry and average bond lengths of 2.40, 2.39, 2.38 and 2.37 Å for **1–4**, respectively. Selected bond lengths for **1–4** are given in Table 2.

We also attempted to incorporate divalent ions such as Zn^{II} or Ni^{II} (square planar) in the place of the Cu^{II} ions as

Table 2. Selected distances [Å] for **1–4**.[a]

	1 (Cu_5Gd_4)	**2** (Cu_5Tb_4)	**3** (Cu_5Dy_4)	**4** (Cu_5Ho_4)
Cu1−O1	1.964(4)	1.949(5)	1.943(4)	1.939(5)
Cu1−O1′	1.964(4)	1.949(5)	1.943(4)	1.939(5)
Cu1−O2	1.978(4)	1.973(5)	1.973(4)	1.976(6)
Cu1−O2′	1.978(4)	1.973(5)	1.973(4)	1.976(6)
Cu2−O16	1.910(5)	1.899(5)	1.908(5)	1.903(6)
Cu2−O15	1.907(5)	1.911(5)	1.913(5)	1.912(6)
Cu2−O1	1.932(4)	1.941(5)	1.927(5)	1.930(5)
Cu2−N4	1.997(6)	1.981(6)	1.999(6)	2.001(8)
Cu3−O14	1.914(4)	1.911(5)	1.914(5)	1.907(6)
Cu3−O12	1.920(4)	1.917(5)	1.929(5)	1.928(6)
Cu3−O1	1.945(4)	1.932(5)	1.940(4)	1.930(5)
Cu3−N3	2.009(5)	2.010(6)	2.008(6)	1.999(8)
Ln1−O15′	2.254(5)	2.236(5)	2.222(5)	2.218(6)
Ln1−O14′	2.260(5)	2.243(5)	2.254(5)	2.231(6)
Ln1−O3	2.305(5)	2.274(5)	2.269(5)	2.267(6)
Ln1−O7	2.306(5)	2.310(5)	2.293(5)	2.289(6)
Ln1−O2	2.422(4)	2.406(5)	2.402(5)	2.384(6)
Ln1−O4	2.528(5)	2.511(5)	2.506(5)	2.491(6)
Ln1−O1′	2.557(4)	2.545(5)	2.553(4)	2.539(5)
Ln1−O5	2.574(4)	2.563(5)	2.554(5)	2.531(6)
Ln2−O12	2.249(5)	2.235(5)	2.215(5)	2.209(6)
Ln2−O16	2.258(5)	2.247(5)	2.245(5)	2.235(7)
Ln2−O3	2.305(4)	2.293(5)	2.275(5)	2.269(6)
Ln2−O8	2.361(6)	2.340(5)	2.338(5)	2.307(6)
Ln2−O2	2.428(4)	2.417(5)	2.402(5)	2.384(6)
Ln2−O10	2.501(5)	2.487(5)	2.484(5)	2.471(6)
Ln2−O9	2.499(5)	2.490(6)	2.482(6)	2.463(7)
Ln2−O1	2.726(4)	2.719(5)	2.708(4)	2.709(5)

[a] Symmetry transformation: $'\ -x, 1-y, 1-z$.

diamagnetic "blanks", but were not successful, despite many attempts. The anisotropic lanthanide systems **2–4** complicate the theoretical description of the system and make it computationally much more difficult to simultaneously determine the nature and magnitude of the Cu–Cu, Ln–Ln and Cu–Ln exchange coupling. Replacement with the above ions would have allowed us to independently identify the magnetic behaviour of the Ln^{III} ion and potentially the nature of the coupling to the Cu^{II} ions. Likewise, we attempted to replace the Ln^{III} ions with a diamagnetic ion such as Y^{III} in order to elucidate the Cu···Cu magnetic interactions, again without success.

Magnetic susceptibility data: Solid-state DC magnetic susceptibility data were collected on **1–4** in fields of 0.01, 0.1 and 1 T over the temperature range of 2–300 K, with the samples contained in Vaseline mulls to prevent torquing of crystallites due to magnetic anisotropy. Plots of $\chi_M T$ versus T are shown in Figure 4 for the approximately 0.01 T (low temperature) and 1 T (high temperature) data. The $\chi_M T$ versus T plots for **1–4** in fields of about 0.01, 0.1, and 1 T are shown in Figures S1–S4 of the Supporting Information. All plots display field dependence below about 20 K and this can be explained by the effects of Zeeman interactions due to low-lying excited states, which is a frequently encountered situation in molecules containing a high percentage of Ln^{III} ions. In essence, it arises as a result of weak exchange interactions of typically $J<1\ cm^{-1}$, thus leading to the

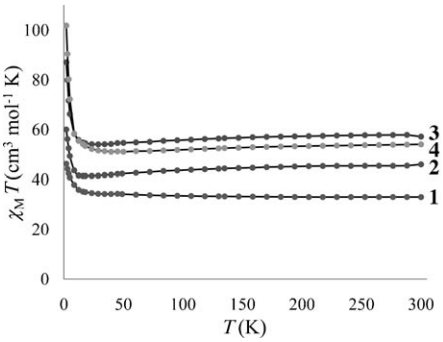

Figure 4. Plots of $\chi_M T$ vs. T for **1** (Cu_5Gd_4), **2** (Cu_5Tb_4), **3** (Cu_5Dy_4) and **4** (Cu_5Ho_4) in a DC field of about 0.01 T (2–70 K) and 1 T (70–300 K). The solid lines are a guide for the eye.

energy separations being very small. It can therefore be assumed that the ground states of **1–4** are very likely near in energy to many other excited spin states.

Compound **1** has a room-temperature $\chi_M T$ value of 33.00 $cm^3 K mol^{-1}$, which is in good agreement with that expected for five uncoupled Cu^{II} ions ($S=1/2$, $g=2$) and four Gd^{III} ions ($S=7/2$, $g=2$) of 33.33 $cm^3 mol^{-1} K$. As the temperature is decreased the $\chi_M T$ value remains constant down to about 30 K. It then increases significantly, at the lowest temperatures and lowest fields measured, to a value of 48.58 $cm^3 mol^{-1} K$, which indicates that ferromagnetic pathways may be present. The magnetization measurements at 2 K and 5 T for **1** (Figure S5 in the Supporting Information) shows a near-saturation value of 31.28 Nβ. This is lower than the expected value of 33 Nβ if all the ions were ferromagnetically coupled. The value observed may indicate a possible $S=31/2$ ground state, which would suggest that not all interactions are ferromagnetic. Qualitatively, one may be able to rationalize a ground state of $S=31/2$ if the central Cu^{II} is strongly antiferromagnetically coupled to the outer Cu sites in the bow tie (Figure 2). This may occur, as the Cu-(central)-O-Cu(outer) interaction with average bond angle of about 126° will likely be antiferromagnetic and stronger than the outer Cu-O-Cu interactions (average angle of 107°), forcing the four Cu sites to align parallel to each other. The Cu···Gd interactions between the outer Cu ions and the Gd ions is then ferromagnetic, which has been noted for a number of Gd and Cu ions bridged by two O atoms. The Cu···Gd interaction is likely to be weak as is normally expected for exchange with Ln^{III} ions. This may lead to the $S=31/2$ ground state, but will most likely lead to a situation in which lots of energy levels are close in energy, with no well-defined ground state, as observed with no clear saturation in the $\chi_M T$ versus T plot. Our quantitative analysis (see below) did not, however, agree with the above $S=31/2$ hypothesis.

Fitting of the experimental data was attempted by using the MAGPACK[26] package with the $\hat{H}=-\Sigma J_{ij}\hat{S}_i\hat{S}_j$ Hamiltonian augmented by a least-squares fitting routine, with a five-J model for the interactions as specified in Table 3 and using the numbering scheme shown in Figure 5.

Table 3. Exchange interactions considered for **1**.

Interacting ions	Parameter	Interacting pairs
Gd–Cu	J_1	1–5, 2–5, 3–5, 4–5
Gd–Cu	J_1'	1–8, 1–9, 2–6, 2–7, 3–6, 3–7, 4–8, 4–9
Cu–Cu	J_2	5–6, 5–7, 5–8, 5–9
Cu–Cu	J_3	6–7, 8–9
Gd–Gd	J_4	1–2, 3–4

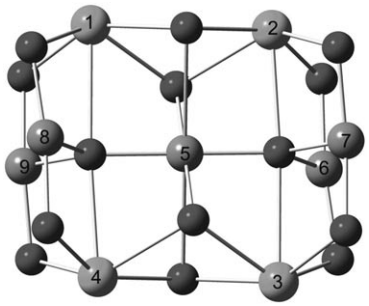

Figure 5. Structural model of the $Cu^{II}_5Ln^{III}_4$ core. Numbers 1–4 represent the Ln^{III} ions, and 5–9 the Cu^{II} ions.

Although many fits could be found to reproduce the rather featureless $\chi_M T$ versus T plot, the values below were the only ones which also reproduced the M versus H data of **1** at 2 K. The fits of $\chi_M T$ versus T and the isothermal M versus H data at 2 K are shown in Figure 6. The following

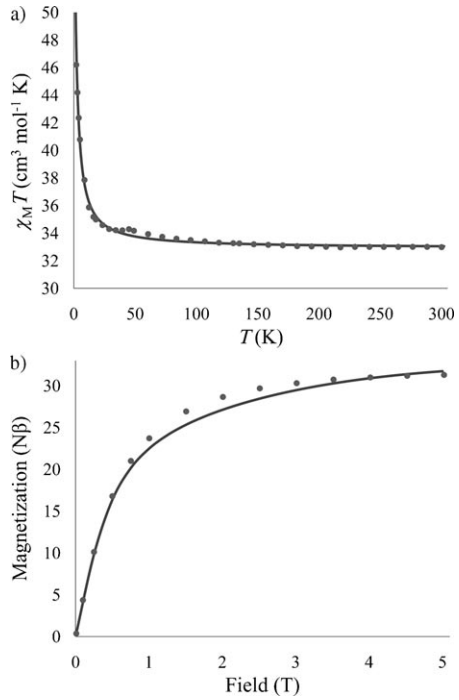

Figure 6. a) $\chi_M T$ vs. T plot for **1** in a DC field of about 0.01 T (2–70 K) and 1 T (70–300 K); the solid line is a fit of the experimental data with the coupling scheme shown in Table 3 and the parameters given in the text. b) Isothermal M vs. H plot at 2 K; the solid line is the fit made with the same parameters as for $\chi_M T$.

magnetic exchange parameter values were obtained and further comments on the fitting procedure are given below: $J_1 = -0.03$, $J'_1 = -0.18$, $J_2 = 0.20$, $J_3 = -0.32$, $J_4 = 0.22\ cm^{-1}$, $g = 1.99$.

With these parameters, the ground state is found to be $S = {}^{23}/_2$, with a large number of excited states $< 1\ cm^{-1}$ above. The Cu(central)-Cu(outer) J_2 was found to be ferromagnetic, different to what we had predicted, whereas the Cu(outer)-Cu(outer) J_3 was found to be antiferromagnetic. The Gd–Cu interaction for **1** was found to be very weak and antiferromagnetic. This was also contrary to what we would have expected. Other satisfactory fits obtained for the $\chi_M T$ versus T data, however, showed this interaction to be weakly ferromagnetic. The nature of the interaction in this case, due to its small value and the complexity of the system, is therefore difficult to determine unambiguously.

In the light of the many potential fits for these data, a rationale for how we came to the above "unique" parameter set is as follows. We recognized that, with five isotropic coupling constants, a cluster "g value" and a large spin basis, the fitting of the magnetic data for **1** was a difficult task. When using a multi-dimensional minimization routine, the choice of initial parameters is often essential in finding a global or local minimum. Hence, many different initial parameter sets were used in an attempt to find an appropriate fit to the $\chi_M T$ versus T curve. These parameter sets led to five different local minima, which were narrowed down to a smaller subset based on prior knowledge of the system involved; that is, the magnitude of the coupling constants involving Gd ions are expected to be small ($< 10\ cm^{-1}$) and the cluster "g value" is expected to be around 2 for ions with no orbital moments. This reduced the number of possible parameter sets to four. The predicted $\chi_M T$ versus T curves were then checked to see if the local minima actually correspond to good fits, which ruled out a further set, leaving three possibilities showing similar $\chi_M T$ versus T curves. These three sets were then used to generate magnetization isotherms which were compared to the experimental magnetization data. Only one parameter set closely resembled the curve, whereas the other two showed poor correlation. The best-fit parameter set for the magnetization was also the best of the three possible sets for the $\chi_M T$ fit, and provided a basis for acceptance of the parameters. Independently, the ab initio study on **3** (see below) determined the Cu–Cu J values to be of the same sign and similar, albeit larger, magnitude, also in contradiction to what was initially predicted and providing further justification for the chosen parameter set for **1**.

Compounds **2–4** have room-temperature $\chi_M T$ values of 45.9, 58.3 and 54.01 $cm^3 mol^{-1} K$, respectively. This is in reasonably good agreement with what is expected for five uncoupled Cu^{II} ions ($S = {}^1/_2$, $g = 2$) and four Tb^{III} ions ($S = 3$, $L = 6$, $^7F_6$, $g = {}^3/_2$, $C = 11.82\ cm^3 mol^{-1} K$)[11c] of 49.15 $cm^3 K mol^{-1}$ for **2**, five Cu^{II} ions ($S = {}^1/_2$, $g = 2$) and four Dy^{III} ions ($S = {}^5/_2$, $L = 5$, $^6H_{15/2}$, $g = {}^4/_3$, $C = 14.17\ cm^3 mol^{-1} K$) of 58.55 $cm^3 mol^{-1} K$ for **3** and five Cu^{II} ions ($S = {}^1/_2$, $g = 2$) and four Ho^{III} ions ($S = 2$, $L = 4$, $^5I_8$, $g = {}^5/_4$, $C =$

14.07 $cm^3 mol^{-1} K$) of 57.78 $cm^3 mol^{-1} K$ for **4**. As the temperature is decreased the $\chi_M T$ value decreases gradually to about 30 K for **2–4** and then increases significantly at the lowest temperatures, with values of 59.98, 87.04 and 101.8 $cm^3 mol^{-1} K$ respectively for **2–4** at 2 K and in a field of 0.01 T. The small decrease of $\chi_M T$ as the temperature is decreased may be due to antiferromagnetic interactions or spin–orbit coupling and crystal-field effects of these ions (depopulation of the Stark sub-levels). The large increase in $\chi_M T$ at very low temperatures as with **1** suggests ferromagnetic interactions may be present, with large-spin ground states for these complexes.

The isothermal magnetization plots for **2–4** (Figure S6–S8 in the Supporting Information) also suggest that large-spin ground states are likely, with values of 22.33, 26.72 and 21.52 Nβ for **2–4**, respectively, at 5 T and 2 K. These plots also reveal a lack of saturation at 5 T and 2 K consistent with the anisotropy of the Ln^{III} ions used and the population of low-lying excited states due to thermal and/or field-induced mechanisms. Again with **2–4** there will be Cu–Cu, Ln–Cu and Ln–Ln magnetic exchange interactions, similar to **1**. The Cu–Cu coupling is again likely to be strongest, whereas the Cu–Ln and Ln–Ln exchanges are expected to be small. One would again expect the Cu–Cu interaction to be antiferromagnetic, and the Cu–Ln interaction ferromagnetic. A more detailed ab initio analysis of the magnetic data for **3** is given below.

Solid-state AC susceptibility measurements in a 5 Oe AC field oscillating at 2000–20 Hz and with a 0 Oe DC field were performed on compounds **1–4** to probe for any SMM behaviour. For compound **1** no out-of-phase signal was detected, which is to be expected due to the isotropic nature of the Gd^{III} ion. These measurements also avoid Zeeman and other effects of a large applied field and are used to determine an estimate of S and the nature (isolated or not) of the ground state. The in-phase χ'_M versus T for **1** displays an increase in $\chi'_M T$ as the temperature is decreased (Figure S9 in the Supporting Information). This would indicate that excited state levels are still populated in this temperature range, with the increase suggesting that excited states of smaller value than the ground state are being depopulated. Extrapolating the $\chi'_M T$ value to 0 K, at which only the ground state will be populated, gives a value of about 60 $cm^3 mol^{-1} K$, which indicates a possible ground state of $S = {}^{21}/_{2}$ or ${}^{23}/_{2}$ depending on g, which is in good agreement with the ground-state value obtained by fitting of the DC data.

Out-of-phase signals are detected for **2–4** below 4 K, with a subsequent decrease of the in-phase signal (less so for **2**), as shown in Figures 7 and 8 for **3** and **4**, respectively, and for **2** in Figure S10 of the Supporting Information. This indicates that **2–4** exhibit slow relaxation of the magnetization and thus probable SMM behaviour. This was to be expected due to the high spin and anisotropic nature of the Ln ions present upon replacement of the Gd^{III} ion. Because no maxima in χ''_M are observed for **2–4**, we are unable to determine the energy barrier U_{eff} and τ_0 via the conventional Arrhenius plot method. Another method, recently employed by Bartolomé et al.,[27] is to assume that there is only one characteristic relaxation process of the Debye type with one energy

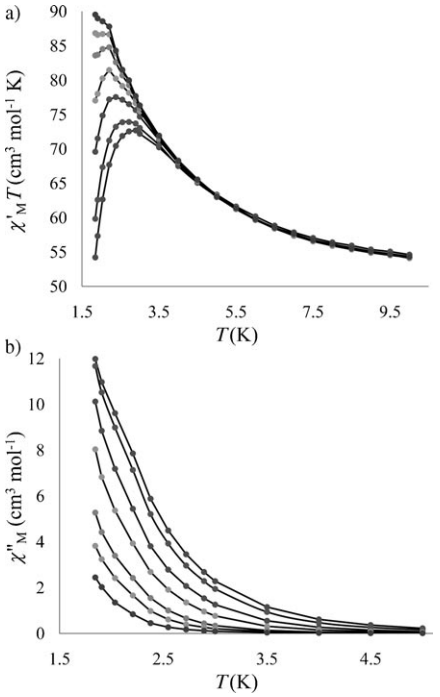

Figure 7. Plots of a) $\chi'_M T$ vs. T (AC frequency, from top to bottom: 20, 50, 100, 250, 500, 100, 1500 Hz) and b) χ''_M vs. T (AC frequency, from top to bottom: 1500, 1000, 500, 250, 100, 50, 20 Hz) for **3**.

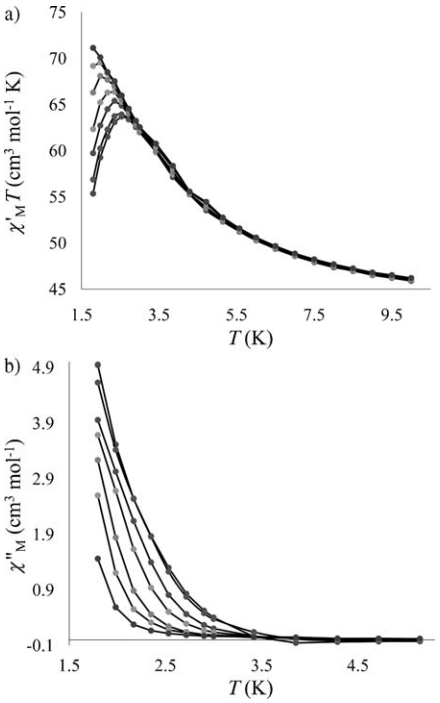

Figure 8. Plots of a) $\chi'_M T$ vs. T (AC frequency, from top to bottom: 20, 50, 100, 250, 500, 1000, 1500 Hz) and b) χ''_M vs. T (AC frequency, from top to bottom: 1500, 1000, 500, 250, 100, 50, 20 Hz) for **4**.

barrier and one time constant. With this assumption, one obtains the following relation [Eq. (1)].

$$\ln(\chi''_M/\chi'_M) = \ln(\omega\tau_0) + E_a/k_BT \quad (1)$$

From this expression, and by plotting $\ln(\chi''_M/\chi'_M)$ versus $1/T$ at the different frequencies, one can perform linear regressions to obtain the gradients (E_a/k_B) and intercepts [$\ln(\omega\tau_0)$] and then extract a estimate of the activation energy and the characteristic time. For **3** (Figure 9), these estimates are

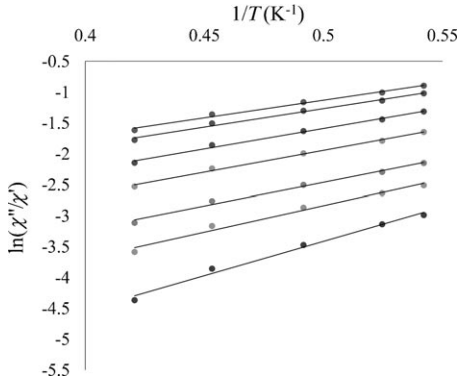

Figure 9. Natural logarithm of the ratio of χ''_M to χ'_M vs. $1/T$ for **3** (AC frequency, from top to bottom: 1500, 1000, 500, 250, 100, 50, 20 Hz).

$U_{eff} \approx E_a = 7 \pm 1$ K and $\tau_0 = (1.3 \pm 0.2) \times 10^{-5}$ s, whereas for **2** and **4** (Figures S11 and S12 in the Supporting Information) the values are $U_{eff} \approx E_a = 11.9 \pm 0.8$ K, $\tau_0 = (9 \pm 6) \times 10^{-6}$ s and $U_{eff} \approx E_a = 10 \pm 4$ K, $\tau_0 = (3 \pm 2) \times 10^{-6}$ s, respectively. To unambiguously confirm SMM behaviour and to obtain more accurate values for U_{eff} and τ_0, single crystal hysteresis studies below 1 K would need to be performed.

Ab initio calculations and exchange coupling for Cu_5Dy_4 complex 3: Due to the limitations of current ab initio methods, local electronic and magnetic properties were studied by employing suitable model fragments for each magnetic centre. Due to inversion symmetry of the Cu_5Dy_4 complex (Figure 1), there are two different Dy sites (Dy1 and Dy2), two different marginal Cu sites (Cu1m and Cu2m), and the central Cu site (Cu3c); see Figures S13 and S15 in the Supporting Information. Ab initio calculations for the dysprosium and copper fragments were performed by using a CASSCF/CASPT2 approach that includes spin–orbit coupling[28] and the magnetic properties ($\chi_M T$ and M) were simulated by a recently developed approach[29] (for further details on the calculations, the Ln and Cu cluster fragments used and the basis sets employed, see the Supporting Information). The Dy^{III} ions are found to be highly anisotropic with $g_z \approx 19.7$ and $g_{x,y} \approx 0$ in the ground Kramers doublet (Table S2 in the Supporting Information). The calculated main anisotropy axes on Dy1 and Dy2 (corresponding to g_z) are almost perpendicular to each other. As a result of this arrangement, the exchange interaction between Dy ions is negligible. The angle between magnetic axes on Dy1 and Dy2 is 86.4°. (Figure S14 in the Supporting Information). The three Cu^{II} sites display typical pseudo-tetragonal type anisotropy with $g_z \approx 2.35$, $g_x \approx 2.1$ and $g_y \approx 2.05$; (Table S4 in the Supporting Information). The ground Kramers doublet on each dysprosium ion is separated from the first excited one by approximately 70 cm^{-1} (see Table S1 in the Supporting Information). Therefore, for the description of low-lying exchange multiplets of the whole Cu_5Dy_4 complex we consider that only the ground Kramers doublet of each Dy^{III} ion is involved in the exchange interaction. The high value of g_z on the dysprosium ions is proof of the essentially axial nature of the ground Kramers doublet.[30] Therefore, the exchange interaction between Dy^{III} centres and neighbouring copper ions will be close to an Ising type.[30] The numbering of the Dy and Cu ions for the exchange model is shown in Figure 5, and the exchange interactions considered, with corresponding J values given in Table 4, afford the following Hamiltonian [Eq. (2)].

$$\begin{aligned}\hat{H}_{exchange} = &-J_1(S_1^{Dy}\cdot S_5^{Cu} + S_1^{Dy}\cdot S_8^{Cu} + S_1^{Dy}\cdot S_9^{Cu} + S_2^{Dy}\cdot S_5^{Cu} + \\ &S_2^{Dy}\cdot S_6^{Cu} + S_2^{Dy}\cdot S_7^{Cu} + S_3^{Dy}\cdot S_5^{Cu} + S_3^{Dy}\cdot S_6^{Cu} + \\ &S_3^{Dy}\cdot S_7^{Cu} + S_4^{Dy}\cdot S_5^{Cu} + S_4^{Dy}\cdot S_8^{Cu} + S_4^{Dy}\cdot S_9^{Cu}) - \\ &J_2(S_5^{Cu}\cdot S_6^{Cu} + S_5^{Cu}\cdot S_7^{Cu} + S_5^{Cu}\cdot S_8^{Cu} + S_5^{Cu}\cdot S_9^{Cu}) - \\ &J_3(S_6^{Cu}\cdot S_7^{Cu} + S_8^{Cu}\cdot S_9^{Cu})\end{aligned} \quad (2)$$

Table 4. Exchange interactions considered for **3**.

Interacting ions	Parameter	Interacting pairs
Dy–Dy	–	
Dy–Cu	J_1	1–5, 1–8, 1–9, 2–5, 2–6, 2–7, 3–5, 3–6, 3–7, 4–5, 4–8, 4–9
Cu–Cu	J_2	5–6, 5–7, 5–8, 5–9
Cu–Cu	J_3	6–7, 8–9

As a result of the perpendicular arrangement of the main anisotropy axes on any Dy–Dy pair (Figure S14 in the Supporting Information), the exchange interaction between the Dy ions is considered negligible. The parameters J_1, J_2 and J_3 are the only fitting parameters used in the model, with the g values being fixed to those obtained by ab initio calculations (Table S2 in the Supporting Information). The exchange interactions were considered within the Lines model, as described elsewhere[29] and included only the ground Kramers doublets of each metal centre. This results in a basis of $2^9 = 512$ exchange functions. The least-squares fit of the magnetic properties on the basis of the ab initio calculated lowest spin–orbit Kramers doublets on the magnetic sites, lead to the following Lines exchange coupling parameters: $J_1 = 1.0$, $J_2 = 1.3$, $J_3 = -4.6$ cm^{-1}.

Thus, the interplay of these Dy–Cu and Cu–Cu exchange interactions is responsible for the magnetism of the complex. The Dy–Cu and Cu(central)–Cu(outer) J_2 interactions are ferromagnetic, whereas the Cu(outer)-Cu(outer) J_3 inter-

actions, with a Cu-O-Cu angle of 107°, are, perhaps surprisingly, antiferromagnetic and stronger, which is also observed in the fit for **1**. The positive J_1 for Dy–Cu in **3** is gratifying in view of our qualitative predictions and the summary of previous studies on Dy–Cu exchange coupling given in the Introduction.

The exchange energies and g tensor values for the ten lowest exchange multiplets, the latter separated by only 1.75 cm^{-1}, are given in the Supporting Information, Table S5. Two views of the arrangement of the local magnetic moments in the ground state of the Cu_5Dy_4 molecule, and the main anisotropy axis of the cluster, are shown in Figure 10. It can be seen that the main anisotropy axis of the complex is almost perpendicular to the Dy_4 plane.

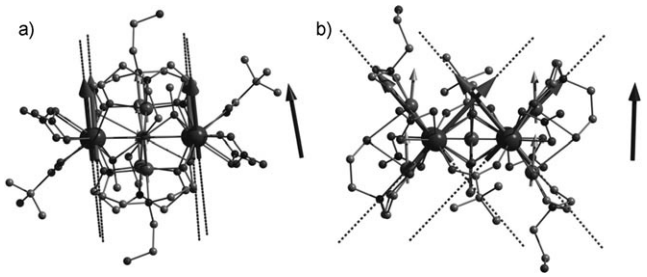

Figure 10. Two views of the arrangement of the local magnetic moments in the ground state of the Cu_5Dy_4 molecule. The arrow outside the cluster shows the main anisotropy axis of the total complex.

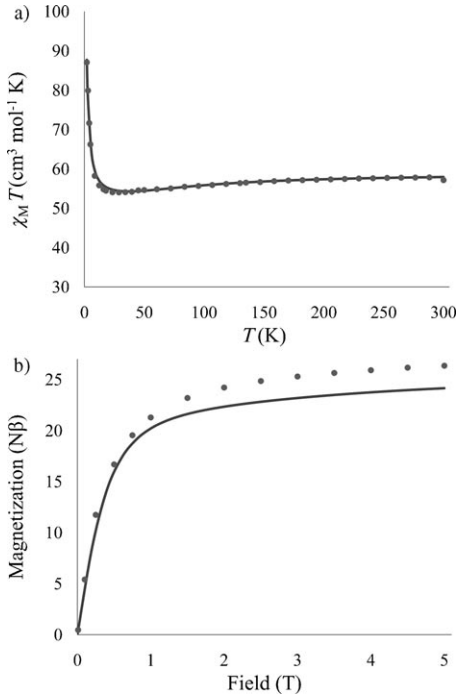

Figure 11. a) Comparison between measured magnetic susceptibility ($\chi_M T$, ●) at applied DC fields of about 0.01 T (2–70 K) and 1 T (70–300 K) and the calculated (——) magnetic susceptibility for **3**. b) Comparison between measured (●) and calculated (——) molar magnetization at 3.0 K for **3**.

The powder $\chi_M T$ data, in fields of 0.01 and 0.1 T, are fitted well, at all temperatures, by the above J values; (Figure 11a). At the higher field of 1 T, the fit is good down to about 25 K, (Figure S16 in the Supporting Information) but does not follow the sharp decrease observed below this temperature, because of Zeeman level (M_S) thermal depopulation effects occurring in this field, as described above, combined with the calculations of $\chi_M T$ being done by using the limit of zero field, on the basis of Van Vleck theory (Supporting Information).

Fitting of the isothermal magnetization M versus H plots using the J values above gave quite good agreement between 0 and 1 T (Figure 11b and Figures S17–S21 in the Supporting Information), but the calculated data between 1 and 5 T at temperatures of 2–20 K were lower by about 10% than the observed values, probably because the first excited Kramers doublet on Dy sites, which are >70 cm^{-1} for both Dy centres (Table S1 in the Supporting Information) should be included in the exchange coupling. However, this would mean that the exchange basis set should contain $4^4 \times 2^5 = 8192$ functions, which is beyond our computational possibilities at this juncture.

Conclusion

We have described the syntheses, structures and magnetism of a new family of heterometallic, nonanuclear Cu^{II}–4f compounds of formulae $[Cu^{II}_5Ln^{III}_4O_2(teaH)_4\{O_2CC(CH_3)_3\}_2(NO_3)_4(OMe)_4]\cdot 2MeOH\cdot 2Et_2O$. Compound **1** (Ln = Gd) displays a combination of ferromagnetic and antiferromagnetic coupling pathways, with no SMM features. On the other hand, inclusion of the anisotropic ions Tb, Dy and Ho in compounds **2**–**4** led to observation of SMM behaviour in their frequency-dependent out-of-phase AC susceptibilities. Ab initio calculations that employ Dy and Cu fragments of cluster **3** and the lowest Kramers levels resulting therefrom yielded good fits of the susceptibility versus temperature behaviour and a corresponding set of best-fit J_1 (Cu–Dy), J_2 (Cu central–Cu outer) and J_3 (Cu outer–Cu outer) values. The first two J values correspond to ferromagnetic pathways and the last-named corresponds to antiferromagnetic pathways. The exchange interaction between Dy ions is negligible due to the perpendicular arrangement of their main anisotropy axes. The main anisotropy axes of the cluster complex is almost perpendicular to the Dy_4 plane.

This combination of experimental work with high-level fragment ab initio calculations gives a clear view of the energy spectrum and magnetic anisotropies on each magnetic centre of the polynuclear cluster. A successful fitting of the experimental magnetic properties on the basis of ab initio calculated local spin-orbital levels, using the Lines parameters as the only fitting parameters of the theory, give a strong argument in favour of the employed approach. This methodology provides a major advance in the interpretation of the DC magnetic susceptibility and isothermal magnetiza-

tion properties of 3d–4f clusters containing anisotropic Ln ions. We have other such 3d–4f and 4f-only clusters in hand to test this approach further.

Experimental Section

All reactions were carried out under aerobic conditions with commercial-grade solvents. Copper(II) nitrate trihydrate, Ln^{III} nitrate hexahydrate, triethanolamine, pivalic acid and triethylamine were obtained from Sigma-Aldrich.

$[Cu^{II}_5Gd^{III}_4O_2(teaH)_4\{O_2CC(CH_3)_3\}_2(NO_3)_4(OMe)_4]\cdot 2MeOH\cdot 2Et_2O$ (1): $Cu(NO_3)_2\cdot 3H_2O$ (0.2 g, 1 mmol) was dissolved in MeOH (20 mL) followed by the addition of triethanolamine (0.13 mL, 1 mmol), pivalic acid (0.05 g, 0.5 mmol) and triethylamine (0.5 mL, 3.5 mmol) to give a green-blue solution. To this solution, $Gd(NO_3)_3\cdot 6H_2O$ (0.45 g, 1 mmol) was added and a deep blue solution resulted. This was stirred for 4 h, allowed to stand and then layered with diethyl ether. After 3–5 d, blue crystals of **1** had formed. Yield: 102 mg, 39.2%. Selected ATR IR data (cm^{-1}): 2957w, 2856s, 1559s, 1483s, 1457sh, 1423s, 1377w, 1360w, 1298s, 1251w, 1227w, 1155w, 1133w, 1083s, 1022s, 916 m, 896 m, 817w; elemental analysis (%) calcd for **1**·2MeOH·2Et_2O ($Cu_5Gd_4C_{48}H_{110}O_{38}N_8$): C 24.49, H 4.71, N 4.76; found: C 24.20, H 4.29, N 4.59.

$[Cu^{II}_5Tb^{III}_4O_2(teaH)_4\{O_2CC(CH_3)_3\}_2(NO_3)_4(OMe)_4]\cdot 2MeOH\cdot 2Et_2O$ (2): As for **1** but $Tb(NO_3)_3\cdot 6H_2O$ (0.44 g, 1 mmol) was used in place of $Gd(NO_3)_3\cdot 6H_2O$. Yield: 120 mg, 46.2%. Selected ATR IR data (cm^{-1}): 2955w, 2859s, 1566s, 1481s, 1458sh, 1424s, 1386w, 1360w, 1294s, 1248w, 1228w, 1155w, 1084s, 1025s, 917 m, 898 m, 817w; elemental analysis (%) calcd for **2**·2MeOH·2Et_2O ($Cu_5Tb_4C_{48}H_{110}O_{38}N_8$): C 24.42, H 4.70, N 4.75; found: C 24.20, H 4.39, N 4.89.

$[Cu^{II}_5Dy^{III}_4O_2(teaH)_4\{O_2CC(CH_3)_3\}_2(NO_3)_4(OMe)_4]\cdot 2MeOH\cdot 2Et_2O$ (3): As for **1** but $Dy(NO_3)_3\cdot xH_2O$ (0.44 g, 1 mmol) was used in place of $Gd(NO_3)_3\cdot 6H_2O$. Yield: 150 mg, 57.6%. Selected ATR IR data (cm^{-1}): 2955w, 2858s, 2385s, 2349s, 2301s, 1566s, 1481s, 1460sh, 1424s, 1384w, 1359w, 1296s, 1248w, 1228w, 1155w, 1085s, 1026s, 916 m, 897 m, 817w; elemental analysis (%) calcd for **3**·2MeOH·2Et_2O ($Cu_5Dy_4C_{48}H_{110}O_{38}N_8$): C 24.27, H 4.67, N 4.72; found: C 24.45, H 4.22, N 4.83.

$[Cu^{II}_5Ho^{III}_4O_2(teaH)_4\{O_2CC(CH_3)_3\}_2(NO_3)_4(OMe)_4]\cdot 2MeOH\cdot 2Et_2O$ (4): As for **1** but $Ho(NO_3)_3\cdot 6H_2O$ (0.44 g, 1 mmol) was used in place of $Gd(NO_3)_3\cdot 6H_2O$. Yield: 124 mg, 47.6%. Selected ATR IR data (cm^{-1}): 2955w, 2858s, 2385s, 2349s, 2301s, 1568s, 1481s, 1461sh, 1424s, 1384w, 1359w, 1296s, 1248w, 1228w, 1154w, 1085s, 1028s, 916m, 897m, 816w; elemental analysis (%) calcd for **4**·2MeOH·2Et_2O ($Cu_5Ho_4C_{48}H_{110}O_{38}N_8$): C 24.17, H 4.65, N 4.70; found: C 24.11, H 4.29, N 4.85.

Physical measurements: Elemental analyses (CHN) were carried out by Campbell Microanalytical Laboratory, University of Otago, Dunedin, New Zealand. IR spectra were recorded on a Bruker Equinox 55 spectrometer with an ATR sampler provided by Specac inc. and the samples were run neat.

X-Ray crystallographic measurements were performed at 100(2) K for **1**, **3** and **4** at the Australian synchrotron MX1 beam-line. The data collection and integration were performed within Blu-Ice[31] and XDS[32] software programs. Data for **2** were collected at 123(2) K on a Bruker Smart Apex X8 diffractometer with $Mo_{K\alpha}$ radiation. Data collection and integration were performed within SMART and SAINT+ software programs, and corrected for absorption using the Bruker SADABS program. Crystallographic data and refinement parameters for **1**–**4** are summarized in Table 1. Structures of **1**–**4** were solved by direct methods (SHELXS-97) and refined (SHELXL-97) by full-matrix least-squares methods on all F^2 data.[33] Crystallographic details are available in CIF format. CCDC 809026 (**1**), 809027 (**2**), 809028 (**3**) and 809029 (**4**) contain the supplementary crystallographic data for this paper. These data can be obtained free of charge from The Cambridge Crystallographic Data Centre via www.ccdc.cam.ac.uk/data_request/cif.

DC magnetic susceptibility measurements were carried out on a Quantum Design MPMS 5 SQUID magnetometer calibrated by use of a standard palladium sample (Quantum Design) of accurately known magnetization or by use of magnetochemical calibrants such as $CuSO_4\cdot 5H_2O$. Microcrystalline samples were dispersed in Vaseline to avoid torquing of the crystallites. The sample mulls were contained in a calibrated gelatine capsule held at the centre of a drinking straw that was fixed at the end of the sample rod. Magnetisation isotherm measurements were made in fields of between 0 and 5 T. AC susceptibilities were measured by using a Quantum Design PPMS instrument with an AC field of 5 Oe and frequencies varying over the range 20 to 2000 Hz at temperatures between 2 and 10 K.

Acknowledgements

This work was supported by a Discovery grant from the Australian Research Council (to K.S.M.). The KU (Leuven) is thanked for financial support (to L.F.C. and L.U.). Structural aspects of this research were undertaken on the MX1 beamline at the Australian Synchrotron, Clayton, Victoria, Australia.

[1] G. Aromi, E. K. Brechin, *Struct. Bonding* **2006**, *122*, 1–67.
[2] E. K. Brechin, *Chem. Commun.* **2005**, 5141–5153.
[3] a) S. Accorsi, A-L. Barra, A. Caneschi, G. Chastanet, A. Cornia, A. C. Fabretti, D. Gatteschi, C. Mortalo, E. Olivieri, F. Parenti, P. Rosa, R. Sessoli, L. Sorace, W. Wernsdorfer, L. Zobbi, *J. Am. Chem. Soc.* **2006**, *128*, 4742–4755; b) A. M. Ako, V. Mereacre, Y. Lan, W. Wernsdorfer, R. Clerac, C. Anson and A. K. Powell, *Inorg. Chem.* **2010**, *49*, 1–3.
[4] a) B. Moubaraki, K. S. Murray, T. A. Hudson, R. Robson, *Eur. J. Inorg. Chem.* **2008**, 4525–4529; b) K. W. Galloway, A. M. Whyte, W. Wernsdorfer, J. Sanchez-Benitez, K. V. Kamenev, A. Parkin, R. D. Peacock, M. Murrie, *Inorg. Chem.* **2008**, *47*, 7438–7442; c) A. Ferguson, A. Parkin, J. Sanchez-Benitez, K. Kamenev, W. Wernsdorfer, M. Murrie, *Chem. Commun.* **2007**, 3473–3475; d) M-H. Zeng, M-X. Yao, H. Liang, W-X. Zhang, X-M. Chen, *Angew. Chem.* **2007**, *119*, 1864–1867; *Angew. Chem. Int. Ed.* **2007**, *46*, 1832–1835; e) Y-Z. Zhang, W. Wernsdorfer, F. Pan, Z-M. Wang, S. Gao, *Chem. Commun.* **2006**, 3302–3304; f) M. Murrie, S. J. Teat, H. Stöckli-Evans, H. U. Güdel, *Angew. Chem.* **2003**, *115*, 4801–4804; *Angew. Chem. Int. Ed.* **2003**, *42*, 4653–4656; g) S. K. Langley, M. Helliweel, R. Sessoli, P. Rosa, W. Wernsdorfer, R. E. P. Winpenny, *Chem. Commun.* **2005**, 5029–5031.
[5] a) A. Ferguson, J. Lawrence, A. Parkin, J. Sanchez-Benitez, K. V. Kamenev, E. K. Brechin, W. Wernsdorfer, S. Hill, M. Murrie, *Dalton Trans.* **2008**, 6409–6414; b) G. Aromí, S. Parsons, W. Wernsdorfer, E. K. Brechin, E. J. L. McInnes, *Chem. Commun.* **2005**, 5038–5040; c) A. Bell, G. Aromí, S. J. Teat, W. Wernsdorfer, R. E. P. Winpenny, *Chem. Commun.* **2005**, 2808–2810; d) S. T. Ochsenbein, M. Murrie, E. Rusanov, H. Stoeckli-Evans, C. Sekine, H. U. Güdel, *Inorg. Chem.* **2002**, *41*, 5133–5140; e) C. Cadiou, M. Murrie, C. Paulsen, V. Villar, W. Wernsdorfer, R. E. P. Winpenny, *Chem. Commun.* **2001**, 2666–2667.
[6] a) A. R. Schake, H-L. Tsai, R. J. Webb, K. Felting, G. Christou, D. N. Hendrickson, *Inorg. Chem.* **1994**, *33*, 6020–6028; b) P. L. Feng, C. C. Beedle, C. Koo, W. Wernsdorfer, M. Nakano, S. Hill, D. N. Hendrickson, *Inorg. Chem.* **2008**, *47*, 3188–3204.
[7] a) C. J. Milios, A. Vinslava, W. Wernsdorfer, S. Moggach, S. Parsons, S. P. Perlepes, G. Christou, E. K. Brechin, *J. Am. Chem. Soc.* **2007**, *129*, 2754–2755; b) R. Inglis, L. F. Jones, C. J. Milios, S. Datta, A. Collins, S. Parsons, W. Wernsdorfer, S. Hill, S. Perlepes, S. Piligkos, E. K. Brechin, *Dalton Trans.* **2009**, 3403–3412; c) C. Milios, S. Piligkos, E. K. Brechin, *Dalton Trans.* **2008**, 1809–1817.
[8] a) P-H. Lin, T. J. Burchell, R. Clerac, M. Murugesu, *Angew. Chem.* **2008**, *120*, 8980–8983; *Angew. Chem. Int. Ed.* **2008**, *47*, 8848–8851; b) J. Tang, I. Hewitt, N. T. Madhu, G. Chastanet, W. Wernsdorfer, C. A. Anson, C. Benelli, R. Sessoli, A. K Powell, *Angew. Chem.*

2006, *118*, 1761–1765; *Angew. Chem. Int. Ed.* **2006**, *45*, 1729–1733; c) Y-Z. Zheng, Y. Lan, C. E. Anson, A. K. Powell, *Inorg. Chem.* **2008**, *47*, 10813–10815; d) M. T. Gamer, Y. Lan, P. Roesky, A. K. Powell, R. Clerac, *Inorg. Chem.* **2008**, *47*, 6581–6583; e) S. K. Langley, B. Moubaraki, C. M. Forsyth, I. A. Gass, K. S. Murray, *Dalton Trans.* **2010**, *39*, 1705–1708; f) B. Hussain, D. Savard, T. J. Burchell, W. Wernsdorfer, M. Murugesu, *Chem. Commun.* **2009**, 1100–1102; g) H. Ke, G-F Xu, L. Zhao, J. Tang, X-Y Zhang, H-J. Zhang, *Chem. Eur. J.* **2009**, *15*, 10335–10338.

[9] For example a) V. Mereacre, A. Ako, R. Clerac, W. Wernsdorfer, I. J. Hewitt, C. E. Anson, A. K. Powell, *Chem. Eur. J.* **2008**, *14*, 3577–3584; b) V. Mereacre, A. Ako, R. Clerac, W. Wernsdorfer, G. Filoli, J. Bartolome, C. E. Anson, A. K. Powell, *J. Am. Chem. Soc.* **2007**, *129*, 9248–9249; c) T. C. Stamatatos, S. J. Teat, W. Wernsdorfer, G. Christou, *Angew. Chem.* **2009**, *121*, 529–532; *Angew. Chem. Int. Ed.* **2009**, *48*, 521–524; d) X-Q. Zhao, Y. Lan, B. Zhao, P. Cheng, C. E. Anson, A. K. Powell, *Dalton Trans.* **2010**, *39*, 4911–4917.

[10] a) P-H Lin, T. J. Burchell, L. Ungur, L. F. Chibotaru, W. Wernsdorfer, M. Murugesu, *Angew. Chem.* **2009**, *121*, 9653–9656; *Angew. Chem. Int. Ed.* **2009**, *48*, 9489–9492; b) Y-N Guo, G-F Xu, P. Gamez, L. Zhao, S-Y Lin, R. Deng, J. Tang, H-J Zhang, *J. Am. Chem. Soc.* **2010**, *132*, 8538–8539; c) I. J. Hewitt, J. Tang, N. T. Madhu, C. E. Anson, Y. Lan, J. Luzon, M. Etienne, R. Sessoli, A. K. Powell, *Angew. Chem.* **2010**, *122*, 6496–6500; *Angew. Chem. Int. Ed.* **2010**, *49*, 6352–6356.

[11] a) A. Bencini, C. Benelli, A. Caneschi, R. Carlin, A. Dei, D. Gatteschi, *J. Am. Chem. Soc.* **1985**, *107*, 8128–8136; b) M. Andruh, I. Ramade, E. Codjovi, O. Guillou, O. Kahn, J. C. Trombe, *J. Am. Chem. Soc.* **1993**, *115*, 1822–1829; c) C. Benelli, D. Gateschi, *Chem. Rev.* **2002**, *102*, 2369–2388.

[12] M. L. Kahn, C. Mathoniere, O. Kahn, *Inorg. Chem.* **1999**, *38*, 3692–3697.

[13] a) T. Kajiwara, M. Nakano, K. Takahashi, S. Takaishi, M. Yamashita, *Chem. Eur. J.* **2011**, *17*, 196–205; b) J-P. Costes, F. Dahan, W. Wernsdorfer, *Inorg. Chem.* **2006**, *45*, 5–7; c) T. Kajiwara, M. Nakano, S. Takaishi, M. Yamashita, *Inorg. Chem.* **2008**, *47*, 8604–8606; d) T. Kajiwara, K. Takahashi, T. Hiraizumi, S. Takaishi, M. Yamashita, *Polyhedron* **2009**, *28*, 1860–1863.

[14] A. J. Blake, R. O. Gould, C. M. Grant, P. E. Y. Milne, S. Parsons, R. E. P. Winpenny, *J. Chem. Soc. Dalton Trans.* **1997**, 485–496.

[15] a) F. Mori, T. Nyui, T. Ishida, T. Nogami, K-Y. Choi, H. Nojiri, *J. Am. Chem. Soc.* **2006**, *128*, 1440–1441; b) A. Okazawa, T. Nogami, H. Nojiri, T. Ishida, *Inorg. Chem.* **2008**, *47*, 9763–9765.

[16] a) J-P. Costes, S. Shova, W. Wernsdorfer, *Dalton Trans.* **2008**, 1843–1849; b) S. Osa, T. Kido, N. Matsumoto, N. Re, A. Pochaba, J. Mrozinski, *J. Am. Chem. Soc.* **2004**, *126*, 420–421; c) S. Ueki, A. Okazawa, T. Ishida, T. Nogami, H. Nojiri, *Polyhedron* **2007**, *26*, 1970–1976; d) T. Hamamatsu, K. Yabe, M. Towatari, S. Osa, N. Matsumoto, N. Re, A. Pochaba, J. Mrozinski, J-L. Gallani, A. Barla, P. Imperia, C. Paulsen, J-P. Kappler, *Inorg. Chem.* **2007**, *46*, 4458–4468.

[17] a) Y. Kobayashi, S. Ueki, T. Ishida, T. Nogami, *Chem. Phys. Lett.* **2003**, *378*, 337–342; b) S. Ueki, T. Ishida, T. Nogami, K-Y Choi, H. Nojiri, *Chem. Phys. Lett.* **2007**, *440*, 263–267.

[18] G. Novitchi, W. Wernsdorfer, L. F. Chibotaru, J-P. Costes, C. E. Anson, A. K. Powell, *Angew. Chem.* **2009**, *121*, 1642–1647; *Angew. Chem. Int. Ed.* **2009**, *48*, 1614–1619.

[19] C. Aronica, G. Pilet, G. Chastanet, W. Wernsdorfer, J-F. Jacquot, D. Luneau, *Angew. Chem.* **2006**, *118*, 4775–4778; *Angew. Chem. Int. Ed.* **2006**, *45*, 4659–4662.

[20] V. Baskar, K. Gopal, M. Helliwell, F. Tuna, W. Wernsdorfer, R. E. P. Winpenny, *Dalton Trans.* **2010**, *39*, 4747–4750.

[21] For example a) K. G. Alley, A. Mukherjee, R. Clerac, C. Boskovic, *Dalton Trans.* **2008**, 59–63; b) J-J. Zhang, S-M. Hu, S-C. Xiang, T. Sheng, X-T. Wu, Y-M. Li, *Inorg. Chem.* **2006**, *45*, 7173–7181.

[22] a) S. K. Langley, K. J. Berry, B. Moubaraki, K. S. Murray, *Dalton Trans.* **2009**, 973–982; b) S. K. Langley, B. Moubaraki, K. J. Berry, K. S. Murray, *Dalton Trans.* **2010**, *39*, 4848–4855; c) S. K. Langley, N. F. Chilton, M. Massi, B. Moubaraki, K. J. Berry, K. S. Murray, *Dalton Trans.* **2010**, *39*, 7236–7248.

[23] a) S. K. Langley, B. Moubaraki, K. S. Murray, *Dalton Trans.* **2010**, *39*, 5066–5069; b) N. F. Chilton, S. K. Langley, B. Moubaraki, K. S. Murray, *Chem. Commun.* **2010**, *46*, 7787–7789.

[24] J. Rinck, G. Novitchi, W. Van den Heuvel, L. Ungur, Y. Lan, W. Wernsdorfer, C. E. Anson, L. F. Chibotaru, A. K. Powell, *Angew. Chem.* **2010**, *122*, 7746–7750; *Angew. Chem. Int. Ed.* **2010**, *49*, 7583–7587.

[25] S. K. Langley, N. F. Chilton, B. Moubaraki, T. Hooper, E. K. Brechin, M. Evangelisti, K. S. Murray, *Chem. Sci.*, **2011**, *2*, 1166–1169.

[26] a) J. J. Borrás-Almenar, J.-M. Clemente-Juan, E. Coronado, B. S. Tsukerblat, *Inorg. Chem.* **1999**, *38*, 6081–6088; b) J. J. Borrás-Almenar, J.-M. Clemente-Juan, E. Coronado, B. S. Tsukerblat, *J. Comput. Chem.* **2001**, *22*, 985–991.

[27] J. Bartolomé, G. Filoti, V. Kuncser, G. Schinteie, V. Meracre, C. E. Anson, A. K. Powell, D. Prodius, C. Turta, *Phys. Rev. B* **2009**, *80*, 014430.

[28] F. Aquilante, L. De Vico, N. Ferre, G. Ghigo, P. A. Malmqvist, P. Neogrady, T. B. Pedersen, M. Pitonak, M. Reiher, B. O. Roos, L. Serrano-Andres, M. Urban, V. Veryazov, R. Lindh, *J. Comput. Chem.*, **2010**, *31*, 224–247.

[29] a) L. F. Chibotaru, L. Ungur, C. Aronica, H. Elmoll, G. Pilet, D. Luneau, *J. Am. Chem. Soc.* **2008**, *130*, 12445–12455; b) L. Ungur, W. Van den Heuvel, L. F. Chibotaru, *New J. Chem.* **2009**, *33*, 1224–1230.

[30] a) W. Van den Heuvel, L. F. Chibotaru, *Phys. Rev. B,* **2010**, *82*, 174436, 1–14;; b) A. Soncini, L. F. Chibotaru, *Phys. Rev. B* **2008**, *77*, 220406; c) D. Visinescu, A. M. Madalan, M. Andruh, C. Duhayon, J.-P. Sutter, L. Ungur, W. Van den Heuvel, L. F. Chibotaru, *Chem. Eur. J.* **2009**, *15*, 11808–11814.

[31] T. M. McPhillips, S. E. McPhillips, H. J. Chiu, A. E. Cohen, A. M. Deacon, P. J. Ellis, E. Garman, A. Gonzalez, N. K. Sauter, R. P. Phizackerley, S. M. Soltis, P. Kuhn, *J. Synchrotron Radiat.* **2002**, *9*, 401–406.

[32] W. Kabsch, *J. Appl. Crystallogr.* **1993**, *26*, 795–800.

[33] a) G. M. Sheldrick, SHELXL-97, *Program for refinement of crystal structures*, University of Göttingen, Germany, **1997**; b) A. L. Speck, *Acta. Crystallogr. Sect. A* **1990**, *46*, c34.

Received: January 20, 2011
Published online: July 5, 2011

